Astronomy & Astrophysics

Two classes of fast-declining Type Ia supernovae

Suhail Dhawan[1,2,3], B. Leibundgut[1,2], J. Spyromilio[1], and S. Blondin[4]

[1] European Southern Observatory, Karl-Schwarzschild-Strasse 2, 85748 Garching bei München, Germany
  e-mail: sdhawan@eso.org
[2] Excellence Cluster Universe, Technische Universität München, Boltzmannstrasse 2, 85748 Garching, Germany
[3] Physik Department, Technische Universität München, James-Franck-Strasse 1, 85748 Garching bei München, Germany
[4] Aix Marseille Université, CNRS, LAM, Laboratoire d'Astrophysique de Marseille, 13013 Marseille, France

ABSTRACT

We aim to characterise a sample of fast-declining Type Ia supernovae (SN Ia) using their bolometric and near-infrared (NIR) properties. Based on these properties, we find that fast-declining SN Ia separate into two categories based on their bolometric and NIR properties. The peak bolometric luminosity (L_{max}), the phase of the first maximum relative to the optical, the NIR peak luminosity, and the occurrence of a second maximum in the NIR distinguish a group of very faint SN Ia. Fast-declining supernovae show a large range of peak bolometric luminosities (L_{max} differing by up to a factor of ~8). All fast-declining SN Ia with $L_{max} < 0.3 \times 10^{43}$ erg s^{-1} are spectroscopically classified as 91bg-like and show only a single NIR peak. SNe with $L_{max} > 0.5 \times 10^{43}$ erg s^{-1} appear to smoothly connect to normal SN Ia. The total ejecta mass (M_{ej}) values for SNe with enough late time data are $\lesssim 1\,M_\odot$, indicating a sub-Chandrasekhar mass progenitor for these SNe.

Key words. supernovae: general

1. Introduction

Type Ia supernovae (SN Ia) have long been linked with the explosion of a C/O white dwarf (Hoyle & Fowler 1960). Ignition of the white dwarf (WD) can lead to fusion of the C/O to ^{56}Ni releasing enough energy to unbind the progenitor, and through the deposition of the energy released in the radioactive decay of ^{56}Ni to ^{56}Co, and on to ^{56}Fe, power the electromagnetic display of the supernova. This scenario is extremely robust and is supported both by theoretical studies (Hillebrandt & Niemeyer 2000) and observations over many decades, although the exact white dwarf mass and ignition scenario remain the subject of extensive debate.

In the past two decades the study of supernovae has been blessed with a great increase in high quality data through a series of systematic surveys for transients, and extended temporal and wavelength coverage. Dedicated supernova searches have discovered several SN Ia with unusual photometric and spectroscopic properties. Some peculiar SN Ia exhibit fast optical post-peak declines and a deep trough-like feature at ~4200 Å in their maximum light spectra, attributed to Ti II. The prototypical example of this class is SN 1991bg (Filippenko et al. 1992; Leibundgut et al. 1993; Mazzali et al. 1997). Li et al. (2011) show that SN 1991bg-like events comprise a large fraction (15−20%) of the SN Ia population in a volume-limited sample and appear distinct from normal SN Ia in their width-luminosity relationship. Events that are SN 1991bg-like have been shown to prefer elliptical and lenticular galaxies (Howell 2001).

Based on multi-epoch spectra and multi-band optical light curves of a sample of fast-declining, SN 1991bg-like SN Ia, Taubenberger et al. (2008) suggest that this class may have a different physical origin to normal SN Ia. However, the possibility that they are a low-luminosity, fast-declining extension of normal SN Ia cannot be excluded. These SNe show markedly different optical colour evolution and low ^{56}Ni mass values as calculated from UBVRI pseudo-bolometric light curves. The discovery of supernovae with intermediate properties between normal and sub-luminous SN Ia would lend support to the latter hypothesis (Garnavich et al. 2004).

The optical width-luminosity relation for SN Ia (Phillips 1993; Phillips et al. 1999; Burns et al. 2011) shows a notable break for fast-declining objects, namely those whose $\Delta m_{15}(B) > 1.6$. Fast-declining SN Ia are fainter given their $\Delta m_{15}(B)$ and assuming a linear relation, possibly due to the inability of $\Delta m_{15}(B)$ to properly characterise fast-declining SNe because their light curves settle onto a linear magnitude decline at approximately fifteen days past B maximum. Burns et al. (2014) proposed a different ordering parameter, s_{BV}, to improve the treatment of fast-declining objects. This parameter is defined as the epoch at which the $(B − V)$ colour curve is at its maximum value, divided by thirty days. Using this metric, the fast-declining SNe appear less distinct and more as a continuous tail of the distribution of normal SN Ia.

In the near-infrared (NIR), SN Ia are remarkably uniform around maximum (Elias et al. 1981; Meikle 2000; Krisciunas et al. 2004; Folatelli et al. 2010; Dhawan et al. 2015). Although a majority of SN Ia show a homogeneous behaviour around the maximum, there are some clear outliers. Garnavich et al. (2004) report that the 91bg-like SN 1999by is fainter in the NIR (using JHK filters) than the average derived for normal SN Ia in Krisciunas et al. (2004). Subsequent studies find a bi-modality in the NIR light-curve properties of fast-declining SN Ia (e.g. Krisciunas et al. 2009; Folatelli et al. 2010; Kattner et al. 2012; Phillips 2012). Events whose NIR primary maxima occur after B-band maximum ($t_B(max)$) are sub-luminous in all bands compared to normal SN Ia. These sub-luminous SN Ia also tend to lack, or have very weak, second maxima in their NIR

Table 1. SN sample used in this analysis.

SN	$t_B(\mathrm{max})$ (MJD; d)	$\Delta m_{15}(B)$ (mag)	s_{BV}	s_{BV} reference	$t_2(Y)$[1] (d)	$t_2(J)$ (mag)	μ	Distance method[**]	Distance reference	Data reference
SN1999by[*] [2]	51 308.3	1.93	0.46	This paper	N/A	N/A	30.82 ($\pm$0.15)	TF	T13	H02, G04
SN2003gs	52 848.3	1.83	0.49	This paper	$\cdots$	15.3 ($\pm$0.7)	31.65 ($\pm$0.28)	SBF	T01	K09
SN2005bl[*]	53 481.6	1.80	0.39	B14	N/A	N/A	35.14 ($\pm$0.09)	LD		WV08, F15
SN2005ke[*]	53 698.6	1.78	0.41	B14	N/A	$\cdots$	31.84 ($\pm$0.08)	SBF	T01	WV08, C10, F15
SN2006gt[*]	54 003.1	1.66	0.56	B14	$\cdots$	20.2 ($\pm$1.2)	36.43 ($\pm$0.05)	LD		C10
SN2006mr[*]	54 050.2	1.84	0.26	B14	N/A	N/A	31.15 ($\pm$0.23)	SBF	A01	C10
SN2007N[*]	54 124.3	1.79	0.29	B14	N/A	N/A	33.91 ($\pm$0.16)	LD		S11
SN2007ax[*]	54 187.5	1.86	0.36	B14	N/A	N/A	32.20 ($\pm$0.14)	TF	T09	S11
SN2007ba[*]	54 196.2	1.88	0.54	B14	20.0 ($\pm$0.4)	$\cdots$	36.18 ($\pm$0.05)	LD		S11
SN2007on	54 421.1	1.90	0.57	B14	18.7 ($\pm$0.4)	18.2 ($\pm$0.1)	31.45 ($\pm$0.08)	SBF	J03	S11
SN2008R[*]	54 494.3	1.85	0.59	B14	15.5 ($\pm$0.7)	14.1 ($\pm$0.7)	33.73 ($\pm$0.16)	LD		S11
SN2008hs	54 812.1	1.83	0.60	This paper	$\cdots$	14.0 ($\pm$1.0)	34.28 ($\pm$0.13)	LD		F15
SN2009F[*]	54 841.8	1.97	0.33	B14	N/A	N/A	33.73 ($\pm$0.16)	LD		S11
SN2010Y	55 247.5	1.73	0.61	This paper	$\cdots$	$\cdots$	33.44 ($\pm$0.20)	LD		F15
iPTF13ebh	56 622.9	1.79	0.63	H15	19.4 ($\pm$0.2)	17.2 ($\pm$1.5)	33.63 ($\pm$0.16)	LD		H15

Notes. [1] SN Ia with only one maximum are marked as "N/A". Ellipses indicate insufficient data to determine a second maximum. [2] SN Ia in the *SN Ia-faint* sub-group are shown in *italics* (see text). [*] Spectroscopically classified as SN 1991bg-like. [**] Methods for distances to the SN hosts are as follows: LD, luminosity distance (using parameters detailed in the text); TF, Tully-Fisher relation; and SBF, surface brightness fluctuation. We wish to note that 0.16 mag (Jensen et al. 2003) is subtracted from SBF distances from Tonry et al. (2001) to put them on the same scale as Freedman et al. (2001). We wish to note that objects that do not have a luminosity distance presented here are not in the *Hubble* flow, meaning they have $z < 0.01$.

References. A01: Ajhar et al. (2001); T01: Tonry et al. (2001); H02: Höflich et al. (2002); J03: Jensen et al. (2003); G04: Garnavich et al. (2004); K09: Krisciunas et al. (2009); WV08: Wood-Vasey et al. (2008); C10: Contreras et al. (2010); S11: Stritzinger et al. (2011); T09: Tully et al. (2009); T13: Tully et al. (2013); F15: Friedman et al. (2015); H15: Hsiao et al. (2015).

light curves. However, objects that peak in the NIR before $t_B(\mathrm{max})$ have NIR absolute magnitudes comparable to normal SN Ia and show prominent, albeit early, second maxima. Following these results, Hsiao et al. (2015) proposed the definition of "transitional" SNe as fast-declining SN Ia with an NIR maximum before $t_B(\mathrm{max})$.

In this paper we analyse the NIR and bolometric properties of fast-declining SN Ia to determine whether they are an extension of normal SN Ia or a distinct subclass. In Sect. 2 we describe our sample and in Sect. 3 we show that fast-declining SN Ia are found in two distinct groups. In Sects. 4.2 and 4.3 we examine other distinguishing characteristics of the groups. The discussion and conclusions are presented in Sect. 5.

2. Data

We compiled a sample of fast-declining SN Ia with $\Delta m_{15} > 1.6$ from the literature. We did not include objects similar to 2002cx, namely those dubbed "Type Iax" supernovae by Foley et al. (2013). Some Iax SNe are fast-decliners (e.g. SN 2002cx, Li et al. 2003; SN 2005hk, Jha et al. 2006; Phillips et al. 2007; SN 2008ha, Foley et al. 2009) and could have been included in our sample, but the evidence for them being different kinds of explosions is mounting (e.g. Li et al. 2003; Jha et al. 2006). We discuss some of the SN Iax features in the conclusions.

Most of our data is compiled from the Carnegie Supernova Project (CSP; Contreras et al. 2010; Stritzinger et al. 2011) augmented by the CfA supernova survey on PAIRITEL (Wood-Vasey et al. 2008; Friedman et al. 2015). To these objects we added SN1999by (Garnavich et al. 2004) and iPTF13ebh (Hsiao et al. 2015). The objects in our sample and the sources of the data are presented in Table 1.

Our sample contains fifteen SNe. Ten of these SNe are spectroscopically classified as 91bg-like (Garnavich et al. 2004; Folatelli et al. 2013). Seven SNe in our sample show a pronounced NIR second maximum, three of which are spectroscopically 91bg-like (2006gt, 2007ba and 2008R).

For SNe with $z > 0.01$, we used luminosity distances with $H_0 = 70\ \mathrm{km\,s^{-1}\,Mpc^{-1}}$, $\Omega_{\mathrm{m}} = 0.27$ and $\Omega_\Lambda = 0.73$. For nearby SNe with $z < 0.01$ we used independent distances to the host galaxy from the literature. A summary of the methods used for the distances and the references is provided in Table 1.

For SNe observed by the CSP, we used published values of s_{BV}. For other SNe we calculated the s_{BV} from SNooPY (Burns et al. 2011) fits to the data.

3. Luminosity vs. colour-stretch: evidence for two classes of fast-declining supernovae

As has been discussed in Dhawan et al. (2015), the infrared spectral region (JHK) is a significant contributor to the bolometric luminosity of SN Ia. We calculated the pseudo-bolometric light curve by integrating over a $u \rightarrow H$ (UV to NIR, UVOIR) spectral energy distribution (SED) based on monochromatic fluxes derived using the transmission curves for each survey (see Contardo et al. 2000, for a detailed explanation of the method). The light curves were corrected for host-galaxy and Milky-Way extinction. We determined the absolute UVOIR peak luminosity (L_{max}) by fitting a cubic spline to the constructed pseudo-bolometric light curve.

The s_{BV} versus L_{max} relationship (Fig. 1) exhibits two distinct groups amongst the fast-declining SN Ia. One group extends the trend of normal Ia supernovae with lower luminosity having an earlier s_{BV} whereas a second group is detached and appears to follow a different relation. The relation for the faint sub-group has a significantly different slope ($\sim 2\sigma$ level, Table 2). We note that the error in the slope for fitting all SNe as a single group is lower than the two separate sub-groups. However, this is because the total sample size is greater than the comparatively smaller subsamples of the two separate groups.

A simple χ^2 per DoF analysis shows that a fit to two sub-classes, meaning fitting two slopes simultaneously, is favoured (reduced $\chi^2 = 1.03$) compared to a single line fit (reduced $\chi^2 = 1.90$). We also applied the hypothesis testing technique of comparing the logarithm of the Bayesian Evidence (Skilling 2004, ln Z).
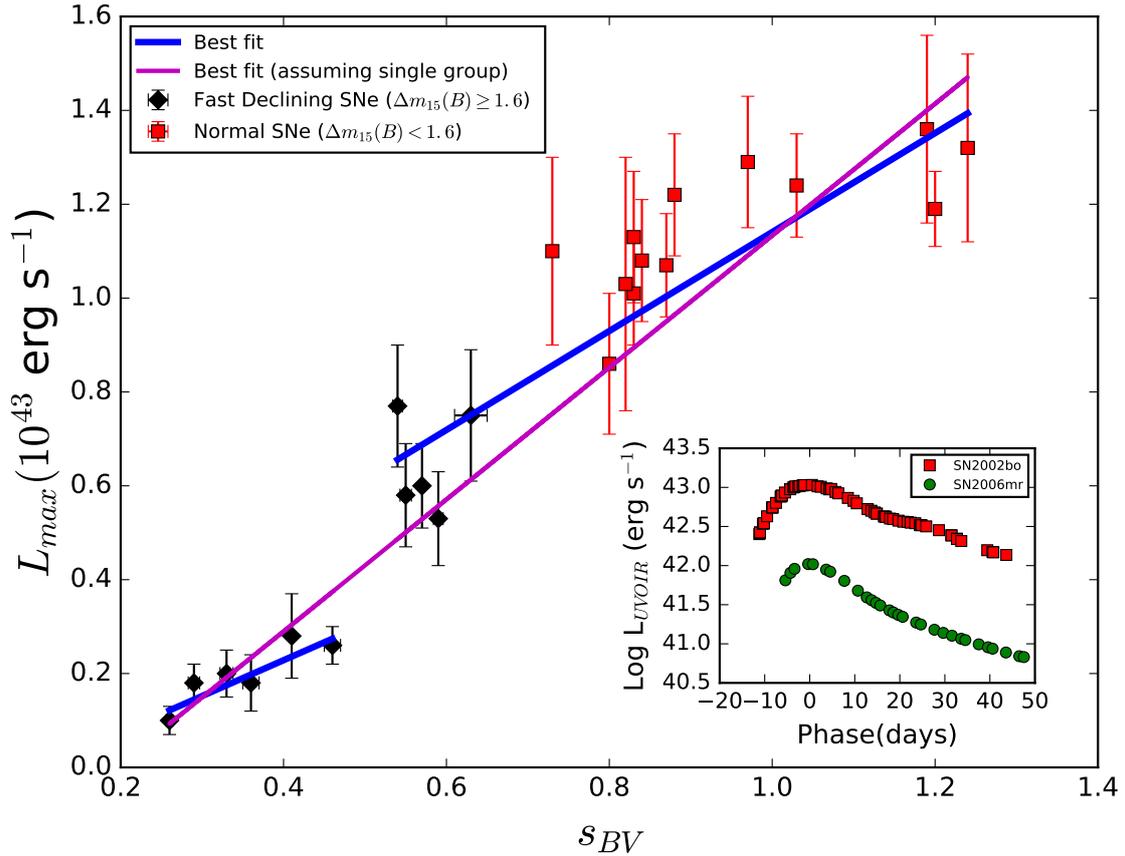
$$Z = \int L\pi \mathrm{d}\theta, \qquad (1)$$

Fig. 1. L_{max} versus s_{BV} for normal SN Ia (red) and fast-declining SN Ia (black). The best-fit linear relations for the faint sub-group of the fast-declining SN Ia, the normal SNe, and the best-fit assuming that all SNe belong to the same group are plotted as solid lines. *Inset*: the $u \rightarrow H$ pseudo-bolometric light curve for SN 2006mr (green), the faintest SN in the sample is plotted in comparison with the normal SN 2002bo (red, Benetti et al. 2004).

Table 2. Slope and intercept for the $L_{max}-s_{BV}$ relation.

Sample	Slope	Intercept
SN Ia-faint	0.76 (±0.17)	−0.08 (±0.06)
Normal SN Ia	1.24 (±0.14)	−0.05 (±0.11)
Complete	1.40 (±0.08)	−0.27 (±0.04)

where L is the likelihood, π is the prior, and θ is the set of the parameters. We calculated $\ln Z$ using a multi-modal nested sampling algorithm, `MultiNest` (Feroz et al. 2013). The $\Delta \ln Z$ for the single population relative to the two subclasses is approximately -6.97, suggesting a strong preference for the two subclasses over the single population. We used the suggestion that $\Delta \ln Z < -5$ is strong evidence for the alternate model over null hypothesis (Trotta 2008). This is an intriguing result, suggesting that there are two separate populations of fast-declining SN Ia, which we refer to as *SN Ia-faint* here, as opposed the group that appears to join the normal SN Ia. The fainter group consists of SNe 1999by, 2005ke, 2006mr, 2007N, 2007ax, and 2009F.

We note that Burns et al. (2014, their Fig. 10) find a the relation between the pseudo-equivalent width of the Si II 5972 Å line and s_{BV} that has a more complicated form than a simple linear relation for SNe with $s_{BV} < 0.5$. This is further evidence that the *SN Ia-faint* sub-group of fast-declining SN Ia are a separate population.

4. Characterising fast-declining, low-luminosity Type Ia supernovae

There appear to be at least three distinguishing characteristics of the *SN Ia-faint* sub-group. In addition to their extreme low luminosity, they appear to reach the NIR peak at a later stage compared to optical wavelengths and do not show a second maximum in their NIR light curves.

4.1. Phase of the first near-infrared maximum

As originally pointed out by Contardo et al. (2000) and extended by future studies (Krisciunas et al. 2004; Kattner et al. 2012; Dhawan et al. 2015), regular SN Ia reach the first maximum in the infrared several days earlier than in the optical bands. The physical reason for this is not entirely obvious, but could be due to the rapid shift of the SED to the blue as the spectrum-formation region heats up (Blondin et al. 2015). Several low-luminosity SN Ia reach their NIR peaks after the optical maximum (Krisciunas et al. 2004; Kattner et al. 2012). We have investigated this for our sample. The magnitude and epoch of the NIR maximum for our sample is reported in Table 3 and displayed against the bolometric peak luminosity in Fig. 2. The separation between the two groups is a function of wavelength and appears to increase from Y to H, with the effect being evident in J and H and less visible in Y. Similar to Fig. 1, the luminosity appears to be the distinguishing property whereas the timing of the

Table 3. Epoch of maximum (with respect to t_B(max)) and peak magnitude in $YJHK$ filters.

SN[1]	t_Y (d)	t_J (d)	t_H (d)	M_Y (mag)	M_J (mag)	M_H (mag)
1999by	...	...	2.98 (±0.63)	...	...	−18.33 (±0.19)
2005bl	...	1.12 (±1.09)	...	...	−17.96 (±0.13)	...
2005ke	1.88 (±0.52)	1.33 (±0.23)	2.05 (±0.28)	−17.42 (±0.08)	−17.45 (±0.08)	−17.50 (±0.08)
2006mr	5.46 (±0.41)	3.26 (±0.12)	5.11 (±0.47)	−17.17 (±0.23)	−17.17 (±0.23)	−17.27 (±0.23)
2007N	6.62 (±1.03)	4.92 (±2.00)	5.96 (±1.30)	−17.48 (±0.16)	−17.48 (±0.18)	−17.65 (±0.21)
2007ax	5.56 (±0.24)	...	4.41 (±1.63)	−17.01 (±0.14)	...	−17.00 (±0.15)
2007ba	1.12 (±0.63)	−1.05 (±1.9)	−0.42 (±1.40)	−18.65 (±0.06)	−18.56 (±0.31)	−18.64 (±0.11)
2007on	−2.88 (±0.10)	−2.67 (±0.10)	−3.49 (±0.10)	−18.28 (±0.19)	−18.37 (±0.19)	−18.18 (±0.19)
2008hs	...	−2.77 (±0.63)	−3.21 (±1.69)	...	−17.96 (±0.15)	−17.82 (±0.15)
2009F	5.14 (±0.90)	1.80 (±1.00)	...	−17.64 (±0.19)	−17.57 (±0.17)	...
2010Y	...	−1.88 (±1.70)	...	...	−18.21 (±0.26)	...
iPTF13ebh	−2.02 (±0.10)	−0.48 (±0.09)	−2.62 (±0.91)	−18.57 (±0.16)	−18.58 (±0.16)	−18.46 (±0.16)

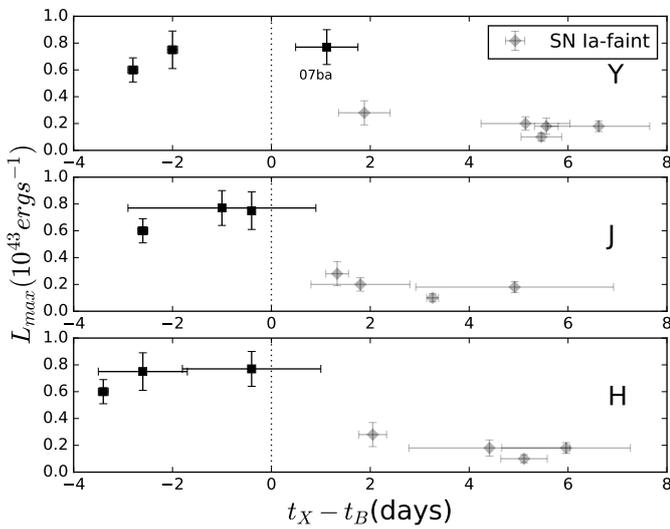**Notes.** [1] SN Ia in the *SN Ia-faint* sub-group are shown in *italics*.

Fig. 2. Pseudo-bolometric peak luminosity versus the timing of the NIR (YJH filters) maximum for SNe in our sample. SNe that peak earlier in the NIR (squares) than the optical also appear to be an extension to the normal SN Ia whereas all SNe with an NIR peak after the optical (diamonds) appear to be a distinct population in Fig. 1.

NIR maximum wrt t_B(max) seems more like a continuous distribution. Nevertheless, the objects in our *SN Ia-faint* sub-group are separated from the normal SN Ia. Additionally, we note that these objects are also sub-luminous in the NIR filters, whereas SNe which peak before t_B(max) are not sub-luminous.

4.2. Lack of a near-infrared second maximum

A further characteristic property of *SN Ia-faint* is the lack of a second infrared maximum. Table 1 indicates the phase of the second maximum for those instances when it could be measured. Objects without a second maximum are labelled "N/A" and correspond to the low-luminosity objects. There is a clear separation of the class of *SN Ia-faint* in this respect. We could not confirm the UVOIR luminosity of SN 2005bl independently, but the lack of a second maximum, the late phase of the first maximum, and a low s_{BV} together indicate that this object also belongs to the *SN Ia-faint* sub-group. Moreover, a low ^{56}Ni mass ($\sim 0.1\ M_\odot$)

from *UBVRI* light-curve calculations by Taubenberger et al. (2008) lends further evidence to its classification as *SN Ia-faint*.

4.3. Low ^{56}Ni and ejecta mass

We can further investigate the properties of fast-declining SN Ia by calculating the ejecta masses and production of ^{56}Ni. From our calculated L_{max}, we estimated the ^{56}Ni mass using:

$$L_{\mathrm{max}} = 2.0(\pm 0.3) \times 10^{43} \frac{M_{^{56}\mathrm{Ni}}}{M_\odot} \mathrm{erg\ s}^{-1}. \qquad (2)$$

This is a simple implementation of Arnett's rule (Arnett 1982; Arnett et al. 1985) for a rise time of nineteen days. Variations in Arnett's rule have been encapsulated in a parameter α (see Branch 1992). We used $\alpha = 1$. Taubenberger et al. (2008) find that fast-declining SN Ia have shorter rise times, typically thirteen to sixteen days, that imply lower ^{56}Ni masses by 40−15 % for the same L_{max}. The resulting ^{56}Ni masses for thirteen and nineteen days rise times are reported in Table 4.

Unsurprisingly, the values of ^{56}Ni mass in Table 4 are significantly lower than the averages derived for normal SN Ia, namely 0.5−0.6 $M_\odot$ (e.g. Stritzinger et al. 2006; Scalzo et al. 2014; Dhawan et al. 2016). The ^{56}Ni mass values we derive range from 0.05−0.38 $M_\odot$, indicating a significant diversity in the sample. A basic assumption in Eq. (2) is that the ejecta mass is the same for all SN Ia when determining a nickel mass. If the *SN Ia-faint* have a lower ejecta mass then the derived nickel masses estimates presented here are too large (Pinto & Eastman 2000). Of course Eq. (2) does not apply if other processes than photon diffusion or a different energy source are at work in low-luminosity SN Ia. We allowed the rise to vary between thirteen and nineteen days in our derivation of the ^{56}Ni mass. The results are presented in Table 4.

To calculate the ejecta mass we used (see Jeffery 1999, for a detailed derivation):

$$M_{\mathrm{ej}} = 1.38 \cdot \left(\frac{1/3}{q}\right) \cdot \left(\frac{v_e}{3000\ \mathrm{km\ s}^{-1}}\right)^2 \cdot \left(\frac{t_0}{36.80\ d}\right)^2 M_\odot. \qquad (3)$$

Equation (3) encapsulates the capture rate of γ-rays in an expanding spherical volume for a given distribution of the radioactive source. The e-folding velocity v_e provides the scaling length for the expansion, and q is a qualitative description of the distribution of the material within the ejecta, with one third

Table 4. ^{56}Ni masses for fast-declining SN Ia with sufficient early time coverage to determine a peak luminosity.

SN[1]	L_{max} (10^{43} erg s^{-1})	$M_{^{56}Ni}$ $t_R = 13$ d; $M_\odot$	$M_{^{56}Ni}$ $t_R = 19$ d; $M_\odot$	$E(B-V)_{host}$ mag	$E(B-V)_{MW}$ mag	R_V[2]	Reference for $E(B-V)_{host}$
1999by	0.26 (±0.04)	0.10 (±0.02)	0.13 (±0.03)	0.020 ±0.030	0.010	3.1	G04
2005ke	0.28 (±0.09)	0.10 (±0.04)	0.14 (±0.04)	0.263 (±0.033)	0.020	1.0	B14
2006gt	0.58 (±0.11)	0.21 (±0.05)	0.29 (±0.07)	0.040 (±0.014)	0.032	3.1	B14
2006mr	0.10 (±0.03)	0.04 (±0.01)	0.05 (±0.02)	0.089 (±0.039)	0.018	2.9	B14
2007N	0.18 (±0.04)	0.07 (±0.02)	0.09 (±0.03)	0.350 (±0.052)	0.034	1.7	B14
2007ax	0.17 (±0.06)	0.07 (±0.02)	0.09 (±0.03)	0.213 (±0.049)	0.045	2.1	B14
2007ba	0.77 (±0.13)	0.28 (±0.06)	0.38 (±0.09)	0.150 (±0.026)	0.032	1.1	B14
2007on	0.60 (±0.09)	0.22 (±0.05)	0.30 (±0.07)	<0.007	0.010	1.9	B14
2008R	0.53 (±0.10)	0.20 (±0.05)	0.27 (±0.07)	0.009 ±0.013	0.062	3.1	B14
2009F	0.20 (±0.05)	0.07 (±0.02)	0.10 (±0.03)	0.108 (±0.047)	0.089	1.0	B14
iPTF13ebh	0.75 (±0.14)	0.28 (±0.07)	0.38 (±0.10)	0.050 (±0.020)	0.067	3.1	H15

Notes. [1] SN Ia in the *SN Ia-faint* sub-group are shown in *italics* . [2] R_V values were calculated using SNooPY fits (Burns et al. 2011, 2014).

References. G04: Garnavich et al. (2004); B14: Burns et al. (2014); H15: Hsiao et al. (2015).

being a uniform distribution and higher values reflecting more centrally-concentrated ^{56}Ni . We assumed a constant γ-ray opacity of 0.025 cm^2 g^{-1} (Swartz et al. 1995).

The "fiducial" timescale (t_0) defined by Jeffery (1999) as a parameter that governs the time-varying γ-ray optical depth behaviour of a supernova is the only "observable". We determined t_0 by fitting the radioactive decay energy deposition to the late time (forty – ninety days) bolometric light curve (see Eq. (4)). Because the UVOIR light curve is not truly bolometric, there is an implicit assumption that the thermal infrared and the ultraviolet beyond the atmosphere cut off are not significant contributors. This assumption is supported by modelling that shows that the infrared catastrophe does not occur until much later and the line-blanketing opacity in the UV remains high (Blondin et al. 2015; Fransson & Jerkstrand 2015). The deposition function for re-processed photons is then given by the following equation:

$$E_{dep} = E_{Ni} + E_{Co,e^+} + [1 - \exp(-\tau)] \cdot E_{Co,\gamma}. \qquad (4)$$

Among the fast-declining SN Ia we have five objects for which we can determine both the maximum bolometric luminosity and the fiducial decay time scale, and thus derive both M_{ej} and $M_{^{56}Ni}$. As described above, the application of Arnett's rule implicitly assumes an ejecta mass through its impact on the diffusion timescale. The rise time of the bolometric light curve is governed by a combination of $M_{^{56}Ni}$ and M_{ej} and, as noted earlier, we attempted to capture any uncertainties in this combination by adopting two rise times for the calculation (thirteen and nineteen days). These rise times were consistently applied also to the determination of M_{ej} . In addition, the fiducial time scale depends on the density structure of the ejecta, which may differ for the fast-declining SN Ia, and thus we explored two different e-folding velocities (2700 km s^{-1} and 3000 km s^{-1}) to represent the range of possible ejecta structures. The least-luminous delayed detonation models of Blondin et al. (2013) have a density profile that is well-characterised by an e-folding velocity of 2500 km s^{-1} whereas the typical value for more luminous models was close to 3000 km s^{-1}(which is similar to the typical e-folding velocity for the sub-M_{Ch} models of Sim et al. 2010). The results are presented in Table 5. We take the range of results to define the uncertainty in our determination of the ejecta mass. The observational error contribution is negligible by comparison. For our analysis, we used $\alpha = 1$. Recent theoretical studies (e.g. Blondin et al. 2013, 2017) find α to be within 20% of

unity. Even for $\alpha = 1.2$, we would obtain a longer transparency timescale, t_0 by ~15%. However, the high values of α imply a more centrally-concentrated ^{56}Ni distribution and hence a higher value for q. Moreover, the high α values correspond to the least luminous models (e.g. Blondin et al. 2013). For SNe corresponding to these luminosities, there is independent evidence for a central concentration of ^{56}Ni such as from low iron line widths in nebular spectra (see Blondin et al. 2012). This implies a significantly higher q value than that assumed here, $q = 1$ compared to $q = 1/3$, that counterbalances the effect of a higher α (see Eq. (3)).

The derived M_{ej} of the *SN Ia-faint* sub-group are a clear indication that these are sub-Chandrasekhar explosions. The highest M_{ej} are found for the shortest rise times and the highest e-folding velocity, meaning the shallowest density structure.

Combining Tables 4 and 5 (for a rise time of thirteen days), we calculated the ratio of the M_{ej} to $M_{^{56}Ni}$ (hereafter, R_M) for fast-declining SN Ia. Fast-declining SN Ia in the *SN Ia-faint* sub-group have significantly larger R_M values compared to normal SN Ia (Fig. 3). An interesting object is SN 2007on, which is the only fast-declining SN Ia connected to the normal SN Ia, displays a $R_M = 4.5$, and is much closer to the value of normal SN Ia with $R_M < 4$. We also show in Fig. 3 the values from different explosion models. The observed ratios of the SN Ia-faint sub-group agree more closely with sub-M_{Ch} model values than with the M_{Ch} values, although the errors are large due to large uncertainties in the individual M_{ej} and $M_{^{56}Ni}$ values.

For longer rise times the derived M_{ej} decrease and the $M_{^{56}Ni}$ estimates increase, which leads to smaller R_M values. In this case, the points tend to drop farther below the line of M_{Ch} explosions.

5. Discussion and conclusions

The ejecta-mass estimates for our SN sample (Table 5) suggest that fast-declining SN Ia are associated with sub-M_{Ch} progenitors. Pure detonations of sub-M_{Ch} WDs have been shown to compare favourably with the narrow light curves of low-luminosity SN Ia and hence reproduce the faint end of the width-luminosity relation (Sim et al. 2010; Blondin 2015; Blondin et al. 2017). One possible mechanism to trigger a sub-MCh WD explosion is the detonation of a surface layer of He, accreted from a companion (e.g. Bildsten et al. 2007), which

Table 5. Fiducial time scales (t_0), ejecta masses (M_{ej}), and bolometric decline rate for the low-luminosity SN Ia with sufficient early and late time coverage to determine a peak luminosity and a late time slope (see text for assumptions about v_e, κ, and q).

| SN	t_0 ($t_R = 13$ d) (d)	t_0 ($t_R = 19$ d) (d)	M_{ej} ($t_R = 13$ d) ($M_\odot$; $v_e = 3000$ km s^{-1})	M_{ej} ($t_R = 13$ d) ($M_\odot$; $v_e = 2700$ km s^{-1})	M_{ej} ($t_R = 19$ d) ($M_\odot$; $v_e = 3000$ km s^{-1})	M_{ej} ($t_R = 19$ d) ($M_\odot$; $v_e = 2700$ km s^{-1})	Decline rate (mag d^{-1})
2005ke	31.69 (±0.83)	28.49 (±0.60)	1.03 (± 0.24)	0.84 (±0.20)	0.83 (±0.20)	0.67 (±0.16)	0.030 (±0.0004)
2006mr	26.72 (±0.47)	24.67 (±0.40)	0.73 (±0.19)	0.61 (±0.17)	0.62 (±0.17)	0.51 (±0.16)	0.039 (±0.0013)
2007ax[1]	28.27 (±0.69)	26.07 (±0.50)	0.81 (±0.21)	0.70 (±0.18)	0.70 (±0.18)	0.56 (±0.16)	...
2007on	29.70 (±0.77)	26.89 (±0.16)	0.90 (±0.21)	0.72 (±0.19)	0.74 (±0.19)	0.60 (±0.16)	0.033 (±0.0003)
2009F[1]	26.49 (±0.60)	24.69 (±0.40)	0.72 (±0.19)	0.60 (±0.16)	0.62 (±0.16)	0.51 (±0.14)	...

Notes. [1] Only using *UBVRI* data.
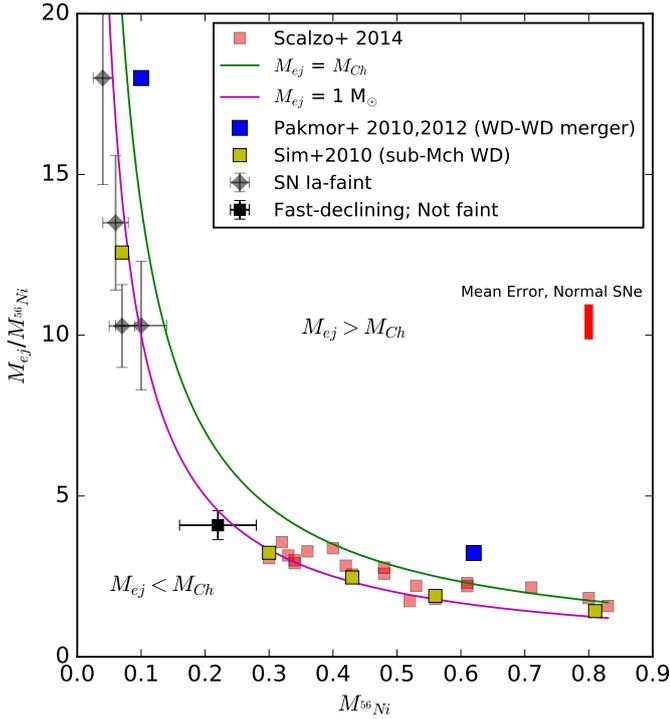
Fig. 3. Ratio of the ejecta mass to ^{56}Ni mass is plotted against the ^{56}Ni mass. With decreasing ejecta mass the black points are SNe 2005ke, 2006mr, 2007on 2007ax and 2009F, the last two of which lack NIR coverage. The diamonds are the *SN Ia-faint* sub-group and the square is 2007on which is fast-declining but not in the sub-group. The red points are normal SN Ia taken from Scalzo et al. (2014). We also plot the values from different model scenarios. The yellow squares are sub-M_{Ch} double detonation models from Sim et al. (2010), blue squares from violent merger models for normal and subluminous SNe from Pakmor et al. (2010, 2012), the green curve is the ratio for a M_{Ch} explosion and the magenta curve is the ratio for a sub-M_{Ch} explosion with M_{ej} of 1 $M_\odot$. We plot the typical error bar for the normal SNe from Scalzo et al. (2014) in red.

in turn triggers a secondary carbon detonation in the WD core (known as the double detonation scenario Woosley & Weaver 1994; Livne & Arnett 1995; Fink et al. 2010; Shen & Moore 2014).

Two SNe in the *SN Ia-faint* sub-group (SN 1999by and SN 2005ke) show significantly larger continuum polarisation (Howell 2001; Howell et al. 2001; Patat et al. 2012) than normal SN Ia (e.g. see Wang et al. 2007; Patat et al. 2009). Detailed modelling of the polarisation spectra of SN 2005ke (Patat et al. 2012) led to the conclusion that the polarisation could arise from one of three scenarios: a WD rotating at close to break-up velocity, a M_{Ch} delayed detonation, or a merger of two WDs. A significantly sub-M_{Ch} ejecta mass (Table 5) combined with the

conclusions from the polarimetry suggest a merger of two WDs, with total mass $M_{tot} < M_{Ch}$ (see van Kerkwijk et al. 2010), to be a possible scenario for SN 2005ke. More spectropolarimetric observations of fast-declining SN Ia will be key to determine their explosion mechanism.

All SNe in the *SN Ia-faint* sub-group are spectroscopically 91bg-like (see Table 1), however three SNe not in this sub-group are also classified as 91bg-like because they show strong Ti II in their maximum light spectra (Folatelli et al. 2013). Therefore, the presence of spectroscopic 91bg-like features is not an exclusive hallmark of the *SN Ia-faint* sub-group, although the Ti II feature in the *SN Ia-faint* sub-group SNe is stronger than the feature in the three SNe not in this sub-group.

The *SN Ia faint* sub-group are characterised by single-peaked NIR light curves. Kasen (2006) find in their lowest ^{56}Ni mass models that the NIR light curves are single-peaked because the shift from doubly- to singly-ionised iron group elements (IGEs) that creates the second maximum occurs only approximately twenty days after explosion, hence coinciding with the primary maximum. Objects in our *SN Ia-faint* sub-group have inferred ^{56}Ni masses $\lesssim 0.1$ $M_\odot$ indicating that their different NIR light-curve morphology is a direct result of the low ^{56}Ni yield. We note that other fast-declining SNe, such as 1991bg, 1998de, show no *i*-band second maximum (Filippenko et al. 1992; Turatto et al. 1996; Modjaz et al. 2001) and a late *i*-band peak, similar to the NIR properties of the *SN Ia-faint* sub-group, which also makes them members of this subclass.

Type Iax supernovae (Foley et al. 2013) also show a single NIR maximum despite displaying a large range of decline rates, $1.2 < \Delta m_{15}(B) < 2.4$, and inferred ^{56}Ni masses, $\sim 0.001 - 0.18$ $M_\odot$. This is understood to be a result of a high degree of mixing of ^{56}Ni seen in three-dimensional deflagration models (e.g. Kromer et al. 2013; Fink et al. 2014) in the ejected material and is observationally-supported by the rapid rise of the light curve to maximum (see e.g. Yamanaka et al. 2015) and the presence of iron in early time-spectra (e.g. Li et al. 2003). The nebular phase spectra of SN Iax, which in some cases show P-Cygni line profiles unlike the forbidden iron lines in nebular spectra of SN Ia (e.g. Jha et al. 2006; Foley et al. 2016), along with the peculiar maximum light spectroscopic and photometric properties, point towards them being distinct explosions from the fast-declining SNe analysed here.

Pure deflagrations that only partially unbind the progenitor to leave a bound remnant (e.g. Kromer et al. 2013, 2015; Fink et al. 2014) can explain the low M_{ej} of the *SN Ia-faint* sub-group, although the corresponding ^{56}Ni masses are higher than the values inferred from observations (Table 4). Pure deflagration models with a significantly lower M_{ej}, ~ 0.2 $M_\odot$, agree well with the *B*-band and bolometric light curves of *SN Ia-faint* sub-group member SN 2005bl (Taubenberger et al. 2008; Fink et al. 2014), but cannot explain the extremely red colours for these SNe. We note, however, that this explosion mechanism would not be a

viable candidate for fast-decliners with two NIR maxima (e.g. SN 2007on) because the ^{56}Ni is highly mixed in the ejecta, producing theoretical light curves with only a single maximum in the NIR.

We show that SN Ia that exhibit s_{BV} below 0.5: deviate from the $L_{\max}$-s_{BV} relation for normal SN Ia; show a low NIR peak luminosity and late NIR maxima; and also lack a prominent second maximum in the NIR filters. This behaviour distinguishes them from fast-declining SN Ia with s_{BV} above 0.5 that seem to extend the normal SN Ia sequence to fainter magnitudes. From this work it is evident that the s_{BV} metric of Burns et al. (2014) is a powerful diagnostic of the nature of the explosion. From the low bolometric luminosity we infer small ^{56}Ni mass and from fitting an energy deposition function to the tail of the bolometric light curve, we infer a sub-$M_{\rm Ch}$ ejecta mass. The low values for these global parameters, combined with the differences in the NIR and bolometric properties of the two sub-groups of fast-declining SN Ia, point to two different explosion scenarios leading to fast-declining SN Ia.

References

Ajhar, E. A., Tonry, J. L., Blakeslee, J. P., Riess, A. G., & Schmidt, B. P. 2001, ApJ, 559, 584

Arnett, W. D. 1982, ApJ, 253, 785

Arnett, W. D., Branch, D., & Wheeler, J. C. 1985, Naturce, 314, 337

Benetti, S., Meikle, P., Stehle, M., et al. 2004, MNRAS, 348, 261

Bildsten, L., Shen, K. J., Weinberg, N. N., & Nelemans, G. 2007, ApJ, 662, L95

Blondin, S. 2015, in Proc. Annual meeting of the French Society of Astronomy and Astrophysics, eds. F. Martins, S. Boissier, V. Buat, L. Cambrésy, P. Petit, 319

Blondin, S., Matheson, T., Kirshner, R. P., et al. 2012, AJ, 143, 126

Blondin, S., Dessart, L., Hillier, D. J., & Khokhlov, A. M. 2013, MNRAS, 429, 2127

Blondin, S., Dessart, L., & Hillier, D. J. 2015, MNRAS, 448, 2766

Blondin, S., Dessart, L., Hillier, D. J., & Khokhlov, A. M. et al. 2017, MNRAS, submitted [arXiv:1706.01901]

Branch, D. 1992, ApJ, 392, 35

Burns, C. R., Stritzinger, M., Phillips, M. M., et al. 2011, AJ, 141, 19

Burns, C. R., Stritzinger, M., Phillips, M. M., et al. 2014, ApJ, 789, 32

Contardo, G., Leibundgut, B., & Vacca, W. D. 2000, A&A, 359, 876

Contreras, C., Hamuy, M., Phillips, M. M., et al. 2010, AJ, 139, 519

Dhawan, S., Leibundgut, B., Spyromilio, J., & Maguire, K. 2015, MNRAS, 448, 1345

Dhawan, S., Leibundgut, B., Spyromilio, J., & Blondin, S. 2016, A&A, 588, A84

Elias, J. H., Frogel, J. A., Hackwell, J. A., & Persson, E. E. 1981, ApJ, 251, L13

Feroz, F., Hobson, M. P., Cameron, E., & Pettitt, A. N. 2013, ArXiv e-print [arXiv:1306.2144]

Filippenko, A. V., Richmond, M. W., Branch, D., et al. 1992, ApJ, 384, L15

Fink, M., Röpke, F. K., Hillebrandt, W., et al. 2010, A&A, 514, A53

Fink, M., Kromer, M., & Seitenzahl, I. R., et al. 2014, MNRAS, 438, 1762

Folatelli, G., Phillips, M. M., Burns, C. R., et al. 2010, AJ, 139, 120

Folatelli, G., Morrell, N., Phillips, M. M., et al. 2013, ApJ, 773, 53

Foley, R. J., Chornock, R., Filippenko, A. V., et al. 2009, AJ, 138, 376

Fransson, C., Jerkstrand, A., Chornock, R., & Filippenko, A. V. 2015, ApJ, 814, L2

Freedman, W. L., Madore, B. F., Gibson, B. K., et al. 2001, ApJ, 553, 47

Friedman, A. S., Wood-Vasey, W. M., Marion, G. H., et al. 2015, ApJS, 220, 9

Foley, R. J., Challis, P. J., Chornock, R., et al. 2013, ApJ, 767, 57

Foley, R. J., Jha, S. W., Pan, Y.-C., et al. 2016, MNRAS, 461, 433

Garnavich, P. M., Bonanos, A. Z., Krisciunas, K., et al. 2004, ApJ, 613, 1120

Hillebrandt, W., & Niemeyer, J. C. 2000, ARA&A, 38, 191

Höflich, P., Gerardy, C. L., Fesen, R. A., & Sakai, S. 2002, ApJ, 568, 791

Howell, D. A. 2001, ApJ, 554, L193

Howell, D. A., Höflich, P., Wang, L., & Wheeler, J. C. 2001, ApJ, 556, 302

Hoyle, F., & Fowler, W. A. 1960, ApJ, 132, 565

Hsiao, E. Y., Burns, C. R., Contreras, C., et al. 2015, A&A, 578, A9

Jeffery, D. J. 1999, ArXiv e-prints [arXiv:astro-ph/9907015]

Jensen, J. B., Tonry, J. L., Barris, B. J., et al. 2003, ApJ, 583, 712

Jha, S., Branch, D., Chornock, R., et al. 2006, AJ, 132, 189

Kasen, D. 2006, ApJ, 649, 939

Kattner, S., Leonard, D. C., Burns, C. R., et al. 2012, PASP, 124, 114

Kromer, M., Fink, M., Stanishev, V., et al. 2013, MNRAS, 429, 2287

Kromer, M., Ohlmann, S. T., Pakmor, R., et al., 2015, MNRAS, 450, 3045

Krisciunas, K., Phillips, M. M., & Suntzeff, N. B. 2004, ApJ, 602, 81

Krisciunas, K., Marion, G. H., Suntzeff, N. B., et al. 2009, AJ, 138, 1584

Leibundgut, B., Kirshner, R. P., Phillips, M. M., et al. 1993, AJ, 105, 301

Li, W., Filippenko, A. V., Chornock, R., et al. 2003, PASP, 115, 453

Li, W., Leaman, J., Chornock, R., et al. 2011, MNRAS, 412, 1441

Livne, E., & Arnett, D. 1995, ApJ, 452, 62

Mazzali, P. A., Chugai, N., Turatto, M., et al. 1997, MNRAS, 284, 151

Meikle, W. P. S. 2000, MNRAS, 314, 782

Modjaz, M., Li, W., Filippenko, A. V., et al. 2001, PASP, 113, 308

Pakmor, R., Kromer, M., Röpke, F. K., et al. 2010, Nature, 463, 61

Pakmor, R., Kromer, M., Taubenberger, S., et al. 2012, ApJ, 747, L10

Patat, F., Baade, D., Höflich, P., et al. 2009, A&A, 508, 229

Patat, F., Höflich, P., Baade, D., et al. 2012, A&A, 545, A7

Phillips, M. M. 1993, ApJ, 413, L105

Phillips, M. M. 2012, PASA, 29, 434

Phillips, M. M., Lira, P., Suntzeff, N. B., et al. 1999, AJ, 118, 1766

Phillips, M. M., Li, W., Frieman, J. A., et al. 2007, PASP, 119, 360

Pinto, P. A., & Eastman, R. G. 2000, ApJ, 530, 757

Scalzo, R., Aldering, G., Antilogus, P., et al. 2014, MNRAS, 440, 1498

Shen, K. J., & Moore, K. 2014, ApJ, 797, 46

Sim, S. A., Röpke, F. K., Hillebrandt, W., et al. 2010, ApJ, 714, L52

Skilling, J. 2004, AIP Conf. Ser., 735, 395

Stritzinger, M., Leibundgut, B., Walch S., & Contardo, G. 2006, A&A, 450, 241

Stritzinger, M. D., Phillips, M. M., Boldt, L. N., et al. 2011, AJ, 142, 156

Swartz, D. A., Sutherland, P. G., & Harkness, R. P. 1995, ApJ, 446, 766

Taubenberger, S., Hachinger, S., Pignata, G., et al. 2008, MNRAS, 385, 75

Turatto, M., Benetti, S., Cappellaro, E., et al. 1996, MNRAS, 283, 1

Tonry, J. L., Dressler, A., Blakeslee, J. P., et al. 2001, ApJ, 546, 681

Trotta, R. 2008, Contemp. Phys., 49, 71

Tully, R. B., Rizzi, L., Shaya, E. J., et al. 2009, AJ, 138, 323

Tully, R. B., Courtois, Hélène, M., Dolphin, A. E., et al. 2013, AJ, 146, 86

van Kerkwijk, M. H., Chang, P., & Justham, S. 2010, ApJ, 722, L157

Wang, L., Baade, D., & Patat, F. 2007, Science, 315, 212

Wood-Vasey, W. M., Friedman, A. S., Bloom, J. S., et al. 2008, ApJ, 689, 377

Woosley, S. E., & Weaver, T. A., 1994, ApJ, 423, 371

Yamanaka, M., Maeda, K., Kawabata, K. S., et al. 2015, ApJ, 806, 191